

# Size distribution of huntite-borate crystals grown by spontaneous crystallization from flux

Valery I. Chani,<sup>a)</sup> Keiji Inoue, Kiyoshi Shimamura, and Tsuguo Fukuda

*Institute for Materials Research, Tohoku University, 2-1-1 Katahira, Aoba-ku, Sendai-shi, 980, Japan*

(Received 21 April 1993; accepted 17 August 1994)

Rare-earth huntite-borates  $R(\text{Al, Ga})_3(\text{BO}_3)_4$ , where  $R = \text{Yb, Er, and/or Nd}$ , were grown by spontaneous crystallization from fluxes based on  $\text{Bi}_2\text{O}_3\text{-B}_2\text{O}_3$ . Crystals were removed from the melts and selected to different size fractions using meshes. It was found that dependence of weight for each size fraction on size in double logarithm coordinates was close to a symmetrical function. The dependence of logarithm of crystal amount on size was almost linear.

Single crystals of borates  $\text{RMe}_3(\text{BO}_3)_4$  with the structure of the natural mineral of huntite  $\text{CaMg}_3(\text{CO}_3)_4$ , where  $R$  represents rare-earth elements or  $\text{Bi}$  and  $\text{Me}$  is  $\text{Al, Cr, and Ga}$ , have applications in nonlinear optics and laser engineering.<sup>1-6</sup> A series of high-melting, chemically inert, and mechanically stable huntite-borate crystals were grown using fluxes based on  $\text{K}_2\text{Mo}_3\text{O}_{10}$ ,<sup>1,2</sup>  $\text{PbO-PbF}_2\text{-B}_2\text{O}_3$ ,<sup>3</sup>  $\text{BaO-B}_2\text{O}_3$ ,<sup>4</sup>  $\text{Bi}_2\text{O}_3\text{-B}_2\text{O}_3$ ,<sup>5-8</sup> and other systems. Tests with a large number of solvents<sup>1-8</sup> led us to the choice of  $\text{Bi}_2\text{O}_3\text{-B}_2\text{O}_3$  as the optimal one for obtaining huntite crystals because in this case the melt system consists of only cations which form huntite structure as host particles.<sup>7</sup>

For preliminary studies of the dependence of optical and crystal-chemical properties on crystal composition, we used a simple crystal growth technique called spontaneous crystallization from a molten flux to give small crystals. In this communication we describe a procedure for growing relatively small single crystals of huntite-borates and discuss the distribution of prepared crystals by size.

Although the study of size distribution of grown crystals was not our main goal, it seems to us that the data obtained are interesting for both fundamental and practical crystal growth.

Four types of charges consisting of crystals and  $\text{Bi}_2\text{O}_3\text{-B}_2\text{O}_3$  flux components were prepared. Melt compositions for runs 5-1, 6-2, 7-1, and 7-2 are given in Table I. Starting materials were (4-9's) oxide powders. Charges were weighed out and fractional amounts were placed in pure platinum crucibles of about 50 ml volume, and the crucibles were placed in a furnace. The furnace temperature was increased to  $T(1)^\circ\text{C}$  over  $t(1)$  h, kept for  $t(2)$  h, and cooled to  $T(2)^\circ\text{C}$  for 30 min. For crystal growth, the melts were cooled slowly from  $T(2)^\circ\text{C}$  to  $T(3)^\circ\text{C}$  during  $t(3)$  h; after that melts with crystals

were cooled to room temperature over 5-10 h. All temperature parameters are given in Table I.

After the crystal growth process, crystals were removed from the melt by dissolving excess flux in hot  $\text{HNO}_3$  and water, and then were dried. The huntite structure for each batch of crystals was checked by x-ray powder diffraction analysis. The grown crystals with the huntite structure were mostly colored transparent hexagonal rods as shown in Fig. 1. Since cooling rates for all melt compositions were too high, the optical quality of the prepared materials was not as high. Moreover, as the given growth procedures shown in Table I were only preliminary ones, other growth parameters also were not optimized. The crystals contained many cracks which were formed during either crystal growth or melt solidification. The as-grown crystals were separated into different size fractions using meshes with hole sizes from 0.037 to 1.680 mm. Each fraction was weighed precisely. The fractions with sizes less than 0.037 mm were not detected. The maximum size of the crystals for all dimensions was about 2.0 mm.

The weights of each fraction for all crystal compositions are presented in Table I. For each fraction with size  $S_i < S < S_{i-1}$ , the size interval  $\Delta S_i$  and the mean size value  $S_i^*$  were calculated using the following formulas:

$$\Delta S_i = S_{i-1} - S_i \quad (1)$$

$$S_i^* = (S_i + S_{i-1})/2 \quad (2)$$

The weights given in Table I were recalculated to wt. % for comparisons between different melts and crystals. In this case, the total weight of crystals for each composition (3) and the weight of crystals with size  $S_i < S < S_{i-1}$  (4) can be represented as follows, respectively:

$$W = \int_0^\infty W(S) dS = 100\% \quad (3)$$

$$W_i = \int_{S_i}^{S_{i-1}} W(S) dS \quad (4)$$

Assuming that the size distribution inside each interval,  $S_i < S < S_{i-1}$ , was linear, it was possible to

<sup>a)</sup>Permanent address: General Physics Institute, Vavilov Street 38, Moscow, 117942, Russia.

TABLE I. Melt compositions (mol %), crystal growth parameters, and weight of each size fraction  $W_i$  ( $S_i < S < S_{i-1}$ ), g for size  $S$  measured in mm.

Melt No.	5-1	6-2	7-1	7-2
Yb <sub>2</sub> O <sub>3</sub>	1.12	0	4.53	0
Er <sub>2</sub> O <sub>3</sub>	2.53	3.69	0	4.58
Nd <sub>2</sub> O <sub>3</sub>	0	0	0.05	0
Bi <sub>2</sub> O <sub>3</sub>	8.29	8.23	8.05	8.11
Al <sub>2</sub> O <sub>3</sub>	5.74	5.78	13.59	13.54
Ga <sub>2</sub> O <sub>3</sub>	5.63	5.81	0	0
Cr <sub>2</sub> O <sub>3</sub>	0	0.27	0	0.15
B <sub>2</sub> O <sub>3</sub>	76.69	76.42	73.78	73.62
$T(1)$ , °C	1200–1250	1300	1300	1300
$T(2)$ , °C	1000	1100	1120	1120
$T(3)$ , °C	600	650	600	600
$t(1)$ , h	9	10	12	12
$t(2)$ , h	7	4	5	5
$t(3)$ , h	96	74	204	204
Yield, wt. %	28	25	38	32
$W_1$ (1.680 < $S$ < 2.0)	0.0172	0.0076	0	0
$W_2$ (1.190 < $S$ < 1.680)	0.3129	0.4589	0	0.0496
$W_3$ (1.000 < $S$ < 1.190)	0.7816	0.6614	0	0.2229
$W_4$ (0.840 < $S$ < 1.000)	1.0973	0.7954	0	0.3199
$W_5$ (0.710 < $S$ < 0.840)	1.7177	1.027	0.2071	0.5201
$W_6$ (0.590 < $S$ < 0.710)	2.9748	1.4388	0.1877	0.5076
$W_7$ (0.420 < $S$ < 0.590)	6.5492	3.3049	0.9704	1.0466
$W_8$ (0.297 < $S$ < 0.420)	5.7232	3.3518	3.2141	1.2299
$W_9$ (0.210 < $S$ < 0.297)	3.2125	2.0322	5.8092	0.9282
$W_{10}$ (0.149 < $S$ < 0.210)	2.435	1.273	6.6528	0.9744
$W_{11}$ (0.088 < $S$ < 0.149)	2.2657	0.6825	5.8417	1.4673
$W_{12}$ (0.074 < $S$ < 0.088)	0.3112	0.0361	0.732	0.285
$W_{13}$ (0.053 < $S$ < 0.074)	0.188	...	0.3586	0.1179
$W_{14}$ (0.037 < $S$ < 0.053)	0.1439	0.0129	0.2725	0.0727
$W_{15}$ (0 < $S$ < 0.037)	0	0	0	0
Total	27.7302	15.0825	24.2461	7.7421

calculate the weight fraction  $W^*$  (wt. %) at the centers of each interval  $S^*$  per  $\Delta S = 0.001$  mm as follows:

$$W_i^*(\text{wt. \%}) = W_i(\text{wt. \%})/\Delta S_i \quad (5)$$

The assumption about linear distribution inside the intervals was reasonable, because the number of meshes used was sufficiently large.

These calculated data are presented in Fig. 2 as  $W^*$  (wt. %) dependence on  $S^*$ . It is interesting to note that using the logarithm axis, the dependence mentioned for all compositions looks like almost symmetrical functions.

It was interesting to represent these data as the dependence of the amount of crystals of each fraction versus size. The length and thickness of the grown crystals (hexagonal rods) were almost equal as shown in Fig. 1. Therefore, for the simplification we assumed that crystals were cubic with size  $S$  and volume  $V = S^3$ . We also assumed that the crystal density was constant because any inclusions in the crystals were not detected using an optical method. Thus, we calculated the total crystal amount in each interval  $\Delta S = 0.001$  mm by a formula:

$$n^* = W^*(\text{wt. \%})/(S^*)^3, \quad (6)$$

where  $n^*$  was measured in relative units. The crystal density should have a constant value at least for the crystals grown from the same melt, because segregation coefficients and crystal compositions could not vary much when the melt cooling rate was constant. The dependence of  $n^*$  on  $S^*$  using only one logarithm axis for the  $n^*$  value is presented in Fig. 3. The dependence of

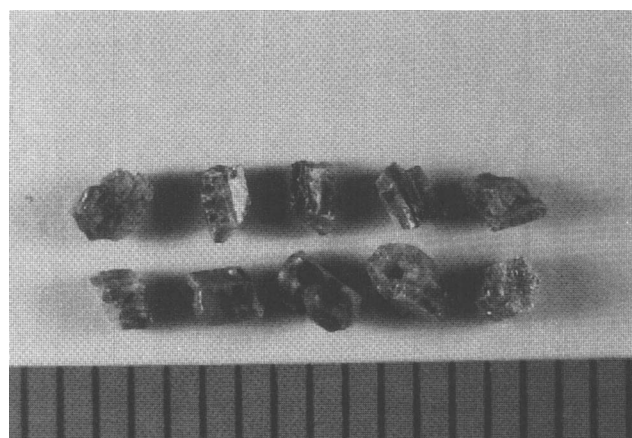


FIG. 1. The shape of 7-2 crystals (1 division = 1 mm).

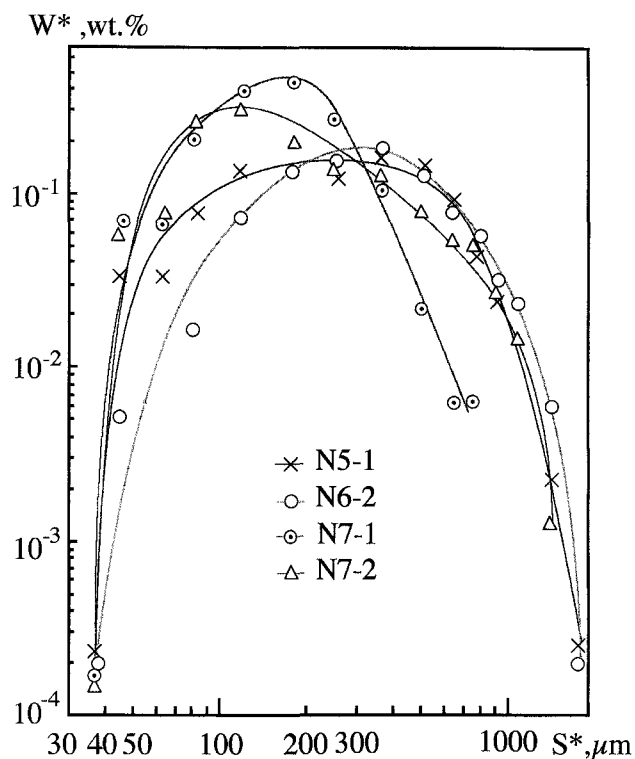


FIG. 2. The dependence of fraction weight  $W^*$  (wt.%) per size interval  $\Delta S = 0.001$  mm on fraction size  $S^*$  for the melts 5-1, 6-2, 7-1, and 7-2.

$n^*$  on  $S^*$  is nearly linear; however, a detailed examination of the data reveals a slight curvature with the size distribution function, because the larger size crystals are more gently sloping. This fact can be explained by the low rate of crystal nucleation at the initial stage of cooling process of the melt, when supercooling was not sufficiently high for mass crystallization. When the supercooling achieved some critical value with further cooling, a lot of crystals were nucleated in the melts. This intensive nucleation continued until the considerable crystal surface area of a large amount of crystals had been formed. After that, the nucleation of new crystals no longer took place because the melt was packed by crystals. The probability of new crystalline aggregates formation decreased, because<sup>9</sup> for the formation of new crystals from crystalline aggregates, the system must overcome a potential barrier  $\Delta\Phi_c$  which has a height

$$\delta\Phi_c = 16\pi\Omega^2 a^3 / 3(\Delta\mu)^2 \quad (7)$$

where  $\Omega$  is the unit volume occupied by atom, molecular, or aggregate in the crystal,  $a$  is the specific free energy of interface, and  $\Delta\mu$  is the difference in chemical potentials of the solid and liquid phases. However, after saturation of the melt by crystalline aggregates it was not necessary to overcome this barrier for further growth of crystals already nucleated. Thus, the nucleation of new crystals halted when the melt was saturated by phase

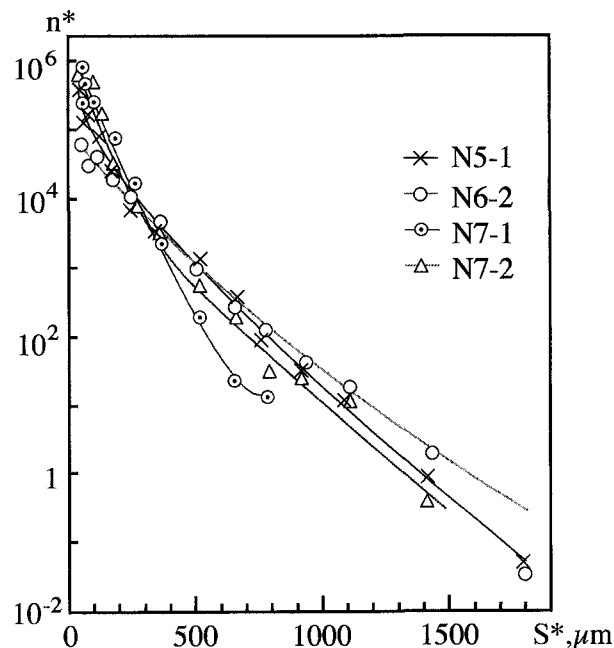


FIG. 3. The dependence of crystal amount  $n^*$  (relative units) on crystal size  $S^*$  per size interval  $\Delta S = 0.001$  mm for the melts 5-1, 6-2, 7-1, and 7-2.

interfaces. That is why the fraction with size  $< 0.037$  mm was not detected.

It is interesting to note that the minimal size crystals were grown from melt 7-1, and the productivity of this melt was highest of the investigated systems. We explain this fact by supposing that within the series of prepared huntite-borates: (5-1):  $(Yb, Er)(Al, Ga)_3(BO_3)_4$ , (6-2):  $Er(Al, Ga)_3(BO_3)_4$ , (7-1):  $YbAl_3(BO_3)_4$ , and (7-2):  $ErAl_3(BO_3)_4$ ,  $YbAl_3(BO_3)_4$  crystals have the minimal interaction energy and the highest stability of crystalline structure. This supposition is based on the known model of structure stability studied for the garnet<sup>10</sup> and huntite<sup>5,6,11</sup> structures.

As it follows from Fig. 2, the geometrical centers  $S^{**}$  of surfaces under each dependence of  $W^*(S^*)$  can be displaced to the direction of high  $S$  values in series as follows:

$$S^{**}(7-1) < S^{**}(7-2) < S^{**}(5-1) < S^{**}(6-2). \quad (8)$$

The crystal lattice interaction energy  $U$  is changed according to the change of the interaction energy of cations, assuming that the interaction energy of  $Yb^{3+}$  with lattice is less than that of  $Er^{3+}$ , and that of  $Al^{3+}$  is less than that of  $Ga^{3+}$ ,<sup>6</sup> as follows:

$$U[YbAl_3(BO_3)_4] < U[ErAl_3(BO_3)_4] < U[(Yb, Er)(Al, Ga)_3(BO_3)_4] < U[Er(Al, Ga)_3(BO_3)_4]. \quad (9)$$

At first sight, the relation of energies (9) between the compositions of 7-2 and 5-1 is not completely correct,

because the cations in both positions were changed. However, although only about 0.5 rare-earth cation per formula unit was changed in the trigonal prism positions, about 1.5 Al<sup>3+</sup> cations per formula unit were replaced by Ga<sup>3+</sup> in the octahedral positions, because the concentrations of Al<sub>2</sub>O<sub>3</sub> and Ga<sub>2</sub>O<sub>3</sub> in melt 5-1 were almost equal. Moreover, some part of rare-earth positions was substituted by Bi<sup>3+</sup> in both compositions. This means that the total amount of replaced rare-earth cations was less than 0.5 cation per formula unit.

Also, we note that the productivity of melts (crystal/melt weight ratio) in the same series decreases regularly in the same order as for (8) and (9) as it follows Table I:

$$P(7-1) > P(7-2) > P(5-1) > P(6-2). \quad (10)$$

This relation is not completely correct and needs further investigations, because the difference between melt compositions achieved 20% of huntite-borate concentration.

It is necessary to note that the fact of decrease of crystal size by the decrease of interaction energy in huntite structure  $U$  needs some explanation. For this reason we suggest the following speculations.

During crystal nucleation the energies of the melt and crystal phases are related by

$$U(\text{huntite}) < U(\text{flux}) \quad (11)$$

because the crystal/flux system is supersaturated and the mass transport process is directed from a liquid phase to a solid one. Thus, in accordance with (9) and (11):

$$U(7-1) < U(7-2) < U(5-1) < U(6-2) < U(\text{flux}) \quad (12)$$

will be valid for similar crystal growth conditions.

However, the chemical potential  $\Delta\mu$  of any phase is equal to energy which is necessary to apply for the change of partial amount in this phase for one unit.<sup>9</sup> Thus, in accordance with (12) it is possible to compare chemical potentials for all compositions investigated. This way the mass exchange between flux and huntite phases is directed by the next relation:

$$[\Delta\mu(7-1)]^2 > [\Delta\mu(7-2)]^2 > [\Delta\mu(5-1)]^2 > [\Delta\mu(6-2)]^2 \quad (13)$$

Taking into consideration formula (7) and assuming that  $\Omega$  and  $a$  values in the same formula are similar for all crystal compositions investigated, potential barriers will be related by:

$$\delta\Phi_c(7-1) < \delta\Phi_c(7-2) < \delta\Phi_c(5-1) < \delta\Phi_c(6-2) \quad (14)$$

As it follows from (9) the number of nuclei formed in unit volume per unit of time  $J$  is equal to:

$$J = B \exp(-\delta\Phi_c/kT) \quad (15)$$

This way, under the condition that the pre-exponential factors are equal for all compositions studied, the rates of nucleation are related as follows:

$$J(7-1) > J(7-2) > J(5-1) > J(6-2) \quad (16)$$

In other words, the total amount  $N$  of more equilibrium crystals is higher than for relatively nonequilibrium ones:

$$N(7-1) > N(7-2) > N(5-1) > N(6-2). \quad (17)$$

An increase of  $N$  parameter means that average size  $S^{**}$  is decreased because all previous reasonings were based on  $W$  parameters calculated in wt. %. The same results were obtained experimentally as it follows from (8).

Thus, when the crystal growth conditions are similar, the potential barrier (7) of the crystals that have a more stable composition for huntite structure is not as high compared with that of the crystals that have a less stable one. Because, since the interaction energy is smaller for the crystals that have a more stable composition for huntite structure, the difference of chemical potentials between the solid and liquid phases,  $\Delta\mu$ , is larger. In this case, the possibility of the nucleation of new crystals is higher.

In summary, the size distribution of huntite-borate crystals was studied. It was found that the dependence of weight for each size fraction on size in double logarithm coordinates was close to a symmetrical function. The dependence of the logarithm of the amount of crystals for each fraction on size was almost linear. It was observed that average size of grown crystals  $S^{**}$  increased with an increase of the interaction energy  $U$ .

## ACKNOWLEDGMENTS

This work was supported by the Japan Society for Promotion of Science (JSPS) and Asahi Glass Foundation.

## REFERENCES

1. N.I. Leonyuk, *Inorg. Mater.* **12**, 482 (1976).
2. N.I. Leonyuk, A.V. Pashkova, and T.I. Timchenko, *Sov. Phys. Dokl.* **24**, 233 (1979).
3. F. Lutz, D. Ruppel, and M. Leiss, *J. Cryst. Growth* **48**, 41 (1980).
4. T.I. Timchenko, N.I. Leonyuk, and G.S. Butusova, *Sov. Phys. Crystallogr.* **25**, 515 (1980).
5. V.I. Chani, K. Shimamura, K. Inoue, and T. Fukuda, *Jpn. J. Appl. Phys.* **32**, 4669 (1993).
6. V.I. Chani, K. Shimamura, K. Inoue, T. Sasaki, and T. Fukuda, *Jpn. J. Appl. Phys.* **33**, 247 (1994).
7. L.N. Brixner and M.S. Licis, *J. Solid State Chem.* **3**, 172 (1971).
8. L.I. Al'shinskaya, N.I. Leonyuk, T.B. Nadezhnaya, and T.I. Timchenko, *Sov. Phys. Dokl.* **24**, 131 (1979).
9. A.A. Chernov, *Modern Crystallography III. Crystal Growth* (Springer-Verlag, Berlin, Heidelberg, New York, Tokyo, 1984).
10. V.I. Chani, *Proc. SPIE 1125, Thin Films in Optics*, 107 (1989).
11. V.I. Chani, K. Shimamura, K. Inoue, T. Fukuda, and K. Sugiyama, *J. Cryst. Growth* **132**, 173 (1993).